Research Square

Preprints are preliminary reports that have not undergone peer review.
They should not be considered conclusive, used to inform clinical practice,
or referenced by the media as validated information.

Automatic Modeling Workpiece Map using Camera and Projector for Automatic Workpiece Alignment Aid of CNC Machining

Wen-Yang Chang

wenyang@nfu.edu.tw

National Formosa University

Jia-Wei Hsu

Zheng-Xun Huang

Hsuan-Jui Chang

Research Article

Keywords: Alignment Aid, Camera–projector System, Structured Light, Intelligent Manufacturing

Posted Date: August 19th, 2026

DOI: https://doi.org/10.21203/rs.3.rs-10672500/v1

License: This work is licensed under a Creative Commons Attribution 4.0 International License.
Read Full License

Automatic Modeling Workpiece Map using Camera and Projector for Automatic Workpiece Alignment Aid of CNC Machining

Wen-Yang Chang[1,2,*], Jia-Wei Hsu[3] ,Zheng-Xun Huang[4], Hsuan-Jui Chang[5]

[1]National Formosa University, Department of Mechanical and Computer-Aided Engineering, Yunlin 632, Taiwan
[2]Smart Machinery and Intelligent Manufacturing Research Center, National Formosa University, Yunlin 632, Taiwan
[3]National Formosa University, Department of Power Mechanical Engineering, Yunlin 632, Taiwan
[4]Doctoral Degree Program in Smart Industry Technology Research and Development, National Formosa University, Yunlin 632. Taiwan
[5]Department of Bioscience and Biotechnology, National Taiwan Ocean University, Keelung, Taiwan

***Corresponding autho**r. E-mail: wenyang@nfu.edu.tw Tel：+886-5-6315325; Address: No.64, Wunhua Rd., Huwei Township, Yunlin County 632, Taiwan

Abstract

During CNC machining, one of the most critical and complex tasks is the establishment of the workpiece coordinate system (work offset), which is typically performed using a tool probe setter. In current industrial practice, this procedure is largely dependent on skilled operators. However, manual operations are prone to human errors, such as incorrect data input or improper probe handling, which may lead to damage to the probe, machine components, or the workpiece. In addition, the accuracy and repeatability of workpiece alignment within the machine coordinate system are essential for ensuring product quality and machining consistency. This study proposes an automatic calibration system for workpiece coordinate setting at the machine home position based on 3D modeling and structured light scanning. The proposed system employs a Gray-code-based structured light method to reconstruct the 3D geometry of the workpiece and to identify edge coordinates for automatic adjustment of the work offset via an optical probe. Experimental results demonstrate that the reconstructed model achieves a dimensional error within ±0.1 mm, while the positioning error based on point cloud edge detection is within 0.05 mm. These results validate the effectiveness and accuracy of the proposed automatic alignment system.

Keywords: Alignment Aid, Camera–projector System, Structured Light, Intelligent Manufacturing

1. Introduction

With the rapid advancement of intelligent manufacturing and the emergence of Industry 4.0, the demand for high-precision and autonomous operation in CNC machining has significantly increased [1-2]. Among various stages in the machining workflow, workpiece alignment plays a crucial role in ensuring machining accuracy, surface integrity, and production efficiency. Traditional alignment methods, including manual adjustment, dial indicators, and touch-trigger probes, are often labor-intensive, time-consuming, and highly dependent on operator experience. These limitations hinder their applicability in modern manufacturing environments characterized by high-mix, low-volume production and the need for rapid reconfiguration.

To address these challenges, vision-based measurement systems have been increasingly adopted due to their non-contact nature, flexibility, and high-speed data acquisition capabilities. Early approaches based on monocular or stereo vision have demonstrated effectiveness in object localization and geometric measurement [3]. However, purely camera-based systems often suffer from sensitivity to ambient illumination, occlusion, and limited depth perception, which restrict their robustness and accuracy in industrial environments. In recent years, structured light techniques have emerged as a powerful solution for high-precision three-dimensional (3D) reconstruction. By projecting coded light patterns onto the object surface and analyzing their deformation, structured light systems enable dense and accurate surface measurement through triangulation principles [4-5]. Compared to alternative 3D sensing technologies, such as laser scanning and time-of-flight sensors, structured light systems offer advantages in terms of accuracy, resolution, and cost-effectiveness [6-7]. Consequently, they have been widely applied in industrial inspection, reverse engineering, and metrology applications.

Recently, event-based calibration [8] and deep learning-based trajectory planning [9] have further enhanced the robustness of these systems in dynamic and reflective industrial environments.

A critical factor influencing the performance of camera–projector systems is calibration accuracy. Numerous studies have proposed various calibration strategies, including geometric modeling methods [10], simplified calibration approaches [11], and self-calibration techniques [12-13]. While these methods improve reconstruction accuracy, many of them require complex procedures, multiple calibration targets, or controlled experimental conditions, which limit their practicality in real-world manufacturing scenarios. To simplify these procedures, high-precision phase mapping [14] and automated board detection [15] methods have been proposed. Furthermore, most existing research focuses on improving measurement accuracy rather than enabling seamless integration with CNC machining systems. Another important challenge lies in the automatic modeling and localization of workpieces within the machining coordinate system. Although structured light has been successfully applied in applications such as tool geometry reconstruction and process monitoring [16], its use for automatic workpiece alignment in CNC environments remains relatively underexplored. Existing approaches often rely on predefined CAD models or require manual initialization, which reduces system autonomy and increases setup time. Therefore, there is a need for a robust and automated solution that can simultaneously perform accurate 3D reconstruction and reliable pose estimation without extensive prior information [17-18].

To bridge this gap, this study proposes an automatic modeling method for generating a workpiece map using a camera–projector system, specifically designed for automatic workpiece alignment in CNC machining [19-20]. The proposed approach integrates structured light projection, image acquisition, and geometric reconstruction to establish a precise mapping between the workpiece and the machine coordinate system. Unlike conventional methods, the proposed system minimizes manual intervention and

eliminates dependence on predefined models, thereby enhancing flexibility and operational efficiency.

The main contributions of this work are summarized as follows. First, an automatic workpiece mapping framework based on a camera–projector system is developed for CNC alignment. Second, a robust feature extraction and registration method is proposed to accurately estimate the workpiece pose. Third, the effectiveness of the proposed approach is validated through experimental implementation, demonstrating improved alignment accuracy and reduced setup time compared with conventional techniques.

2. Methodology

2.1 3D Scanning System Integrated with CNC Machine

It is very complicated and well-known that the CNC operators need to manually set the work-offset distances and to partially operate the optical probe for G54 g-code program before running the CNC machine. Therefore, the study developed a 3D scanning system of intelligent CNC machine to recognize any workpiece dimensions for automatically moving work-offset distance of an optical probe to machine G54 position. The intelligent CNC machine is set on a 5-axis CNC machine tool (model YCM-FV85A with a controller of FANUC 18i-MB5), a 3D scanning system with a micro projector (model Optoma ML330), and a CCD (model Basler ace acA1600-20uc), an optical probe (model Renishaw OMP400), a mini computer that run multiple neural networks in parallel (NVIDIA jetson Nano), and a smart box (SMB), as shown in Fig. 1.

The maximum spindle speed, spindle power, rapid speed, and feed speed of the 5-axis CNC machine tool are 12000 rpm, 7.5 kW, 36 M/min, and 10 M/min, respectively. The contrast ratio, brightness, resolution, maximum bit rate, projected range, and dimension of the micro projector are 20000:1, 600 lm, 1280×800, 30 Mbps, 0.3-3 M, and 157 x 133 x 35 mm^3, respectively. The frame rate, pixel size, resolution, and pixel bit depth of the CCD camera are 20 fps, 4.4 µm x 4.4 µm, 2 MP, and 12 bits, respectively. The accuracy, speed range, length, and stylus over-travel angle of the optical probe are 0.25 µm, 10-100 mm/min, 100 mm, and ±11°, respectively. The stylus trigger forces in XY plane and Z directions are 0.06 N and 2.55 N, respectively. The specifications of the SMB are the Intel Atom X5-Z8350 Soc, 4 GB DDR3L memory, 32 GB eMMC storage, and Gigabit LAN for windows 11 system. This integrated system enables automatic recognition of workpiece dimensions and precise adjustment of the work offset, thereby improving machining efficiency and reducing human intervention. This process is not only time-consuming but also highly dependent on operator experience, which may lead to errors.

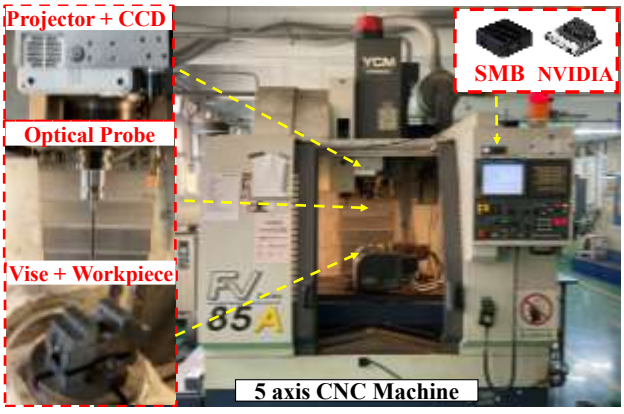


Fig. 1. Intelligent CNC machine based on 3D scanning system to recognize any workpiece dimensions for automatically moving work-offset of optical probe to machine home position.

2.2 Calibrations of scanning system

The 3D workpiece is built using a camera and a projector based on structured light. Fig. 2 shows the system calibrations between the camera and the projector using the printed and projected chessboards, respectively. The calibrations include the intrinsic parameters, extrinsic parameters, and distortion coefficients of the camera itself and the relationship between the camera and the projector using the printed and projected chessboards, respectively.

The printed chessboard that was printed on paper is used to calibrate the intrinsic and extrinsic parameters of the camera itself and is 9×7 regular squares of Gray and white patterns with a square of 30 mm × 30 mm. The projected chessboard that was projected from a mini projector is used to calibrate the intrinsic and extrinsic parameters between the camera and the projector. The matrix size of the projected chessboards is 8×6 regular squares of filling black and white patterns with a square of 75 pixel × 75 pixel.

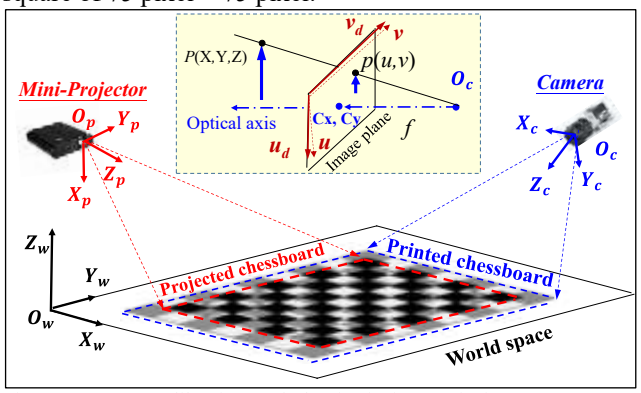


Fig. 2. System calibrations of the intrinsic, extrinsic parameters, and distortion coefficients of the camera itself and the relationship between the camera and the projector using the printed and projected chessboards, respectively.

Without consideration of lens distortion, the coordinate map amount the 2D image plane $[u, v]$, the camera system $[X_C, Y_C, Z_C]$, and the 3D world space $[X_W, Y_W, Z_W]$ is given as eq. (1), where s is a non-zero scale factor and $[u, v, 1]$ is the homogeneous coordinate on the image plane. The superscript symbol k can be substituted for c or p. If k is c that indicated the intrinsic $[A]^c$ and extrinsic $[R|T]^c$ parameters of the camera itself, where R and T are represented the rotation matrix and the translation vector between world and image frames, respectively. In addition, the first column $[r_{xx}, r_{yx}, r_{zx}]^T$ of the R matrix is x, y, and z rotated directions of the x axis. The $[t_x, t_y, t_z]^T$ is the translation distances of x, y, and z direction to the original coordinate of the image plane. If k is p that indicated the intrinsic $[A]^p$ and extrinsic $[R|T]^p$ parameters between the camera and the projector. C_x and C_y are the positions of optical center on image plane. f_x and f_y are the focal lengths in the x and y directions on the image plane, respectively.

$$s\begin{bmatrix}u\\v\\1\end{bmatrix}^k = [A]^k\begin{bmatrix}X_C\\Y_C\\Z_C\end{bmatrix} = [A]^k[R|T]^k\begin{bmatrix}X_W\\Y_W\\Z_W\\1\end{bmatrix}, \quad k = c \text{ or } p \qquad (1)$$

$$\text{where } [A]^k = \begin{bmatrix}f_x & 0 & C_x\\0 & f_y & C_y\\0 & 0 & 1\end{bmatrix}^k, \quad [R|T]^k = \begin{bmatrix}r_{xx} & r_{xy} & r_{zz} & t_x\\r_{yx} & r_{yy} & r_{yz} & t_y\\r_{zx} & r_{zy} & r_{zz} & t_x\end{bmatrix}^k$$

With considering the radial (D_r) and tangential (D_t) distortions of the camera lens, the projective transformation in camera 3D coordinates $[X_C, Y_C, Z_C]$ is required to normalize in the 2D image plane. The study assumed that $[u', v', 1]$ is the normalized coordinate which describes the image distortion due to the optical problem in the image coordinates. The new normalized coordinate after calibrating

the lens distortion is defined as $[u'', v'', 1]$ and the above model is extended as eq. (2)

$$\Rightarrow \frac{s}{Z_c}\begin{bmatrix} u \\ v \\ 1 \end{bmatrix}^k = [A]^k \begin{bmatrix} \frac{X_C}{Z_C} \\ \frac{Y_C}{Z_C} \\ 1 \end{bmatrix} \equiv [A]^k \begin{bmatrix} u' \\ v' \\ 1 \end{bmatrix} = [A]^k \begin{bmatrix} u'' \\ v'' \\ 1 \end{bmatrix} \quad (2)$$

where k is c or p, and $\left[\frac{X_C}{Z_C}, \frac{Y_C}{Z_C}, 1\right]^T = [u', v', 1]^T$

For radial distortion $[D_r]$ and the tangential distortion$[D_t]$

$$\begin{bmatrix} u'' \\ v'' \\ 1 \end{bmatrix} = [D_r] + [D_t]$$

where $[D_r] = \begin{bmatrix} 1 + k_1 r^2 + k_2 r^4 + k_3 r^6 \\ 1 + k_1 r^2 + k_2 r^4 + k_3 r^6 \\ 1 \end{bmatrix} \begin{bmatrix} u' \\ v' \\ 1 \end{bmatrix}$ and

$$[D_t] = \begin{bmatrix} 2p_1 u'v' + p_2(r^2 + 2u'^2) \\ 2p_2 u'v' + p_1(r^2 + 2v'^2) \\ 1 \end{bmatrix}$$

The k_1, k_2, and k_3 are the coefficients of the radial distortion, the p_1 and p_2 are the coefficients of the tangential distortion, and $r^2 = u'^2 + v'^2$.

In order to calibrate the coordinate relationship between the any point P(X,Y,Z) of the world space and any point p(u,v) of the real image plane, the camera firstly captures 15 images of the printed chessboard that were placed at different poses to automatically obtain all coefficients of the intrinsic $[A]^c$ and extrinsic $[R|T]^c$ parameters of the camera itself, as shown in table 1. Similarly, in order to calibrate the coordinate relationship between the camera (X_c, Y_c, Z_c) and the projector (X_p, Y_p, Z_p), the projector projected 15 different poses of the chessboard patterns on the different poses of the printed chessboard. Then, the camera sequentially captures these 15 images of the projected chessboards to calibrate all coefficients of the intrinsic $[A]^p$ parameters, and extrinsic $[R|T]^p$ parameters between the camera and the projector, as shown in table 1.

Table 1. Calibrated results for intrinsic and extrinsic parameters of the camera and projector

Parameters	Camera	Projector
Intrinsic matrix $[A]$	$\begin{bmatrix} 1845.588 & 0 & 790.971 \\ 0 & 1842.396 & 579.472 \\ 0 & 0 & 1 \end{bmatrix}^c$	$\begin{bmatrix} 1563.924 & 0 & 614.861 \\ 0 & 1999.161 & 1030.081 \\ 0 & 0 & 1 \end{bmatrix}^p$
Extrinsic matrix $[R\|T]$	$\left[\begin{array}{ccc\|c} -0.0055 & 0.9999 & -0.0121 & -172.482 \\ 0.977 & 0.0029 & -0.213 & -120.004 \\ -0.2129 & -0.013 & -0.9769 & 700.338 \end{array}\right]^c$	$\left[\begin{array}{ccc\|c} -0.006 & 0.9999 & -0.0089 & -84.493 \\ 0.9996 & 0.0057 & -0.024 & -227.851 \\ -0.024 & -0.0091 & -0.9996 & 645.047 \end{array}\right]^p$
Distortion coefficients $[k_1, k_2, k_3, p_1, p_2]$	[-0.0425, 0.061, 0,-0.0013, -0.0037] ^{c}	[0.0068, -0.209, 0,-0.0023, -0.0029] ^{p}

2.3 Projective procedures of structured light

After calibrations of the scanning system, a mini projector projected several Gray structured lights on workpiece surface for capturing images with a camera. Generally, the inter-reflections, diffusion and sub-surface scattering easily degrade the 3D modeling performance of structured light scanning due to light effects. Especially, the metal surfaces are easily to cause light reflection when the conventional Gray code is projected on metal surface. This study modified the projective patterns of conventional structured light that added an inverse Gray code to reduce the reflection effect on metal surface.

In this study, the projective procedures of structured light in column direction were shown in Fig. 3 that included (a) generated binary codes of B1 to B10, (b) bitwise XOR operation to Gray codes of G1 to G10, (c) inverse Gray codes to form $\overline{G1}$ to $\overline{G10}$, and (d) integrated cross codes of G and $\overline{G}$. The projected numbers N included the column N_{col} and the row N_{row} directions of the integrated cross codes patterns, an all-white pattern, and an all-black pattern as eq. (3):

$$N = 2(N_{col} + N_{row}) + 2 = 2(\log_2 w + \log_2 h) + 2 \quad (3)$$

where the w and h are the width and height resolutions of the projector, respectively. The resolution of the projector is 1024 and 768 pixels indicated that N_{col} and N_{row} are both 10 patterns calculated round up values. Two reference images of all-white and all-black patterns are used to estimate the object brightness that the average intensity of the all-white and all-black patterns after projecting patterns on the object could be used to assign as threshold of depth decoding.

For generating B1 to B10 binary patterns in column direction as shown in Fig. 3(a), the strip widths of the sequential projection are generated from low frequency to high frequency per screen. The frequencies of B1 to B10 strip widths are 1 to 512 periods per screen in this study. The low frequency patterns could eliminate short-range indirect effects of sub-surface scattering and defocus. In order to minimize errors during image scanning, the binary code will be converted to Gray codes of G1 to G10 using bitwise XOR operation, as shown in Fig. 3(b). The high frequency could bypass long-range indirect effects of inter-reflections and diffusion. For generating Gray codes of G1 to G10, the binary patterns are transformed to Gray codes using bitwise XOR operation as eq. (4). Gray code sequences have the property of being able to detect any single-bit coding error because two adjacent codes only change one bit value. Then, to reverse the Gray codes of G1 to G10 to reduce the reflection effect on metal surface, as shown in Fig. 3(c). Finally, the integrated Gray codes of each G and $\overline{G}$ are projected onto the scene to be captured and to be uniquely labeled each pixel, as shown in Fig. 3(d).

$$\text{G1=B1} \oplus \text{B1} \text{ and } \text{Gn} = \sum_{n=2}^{10} \text{B(n+1)} \oplus \text{Bn} \quad (4)$$

First, the B1 pattern of binary code with black and white that is projected on workpiece surface, then projected frequency of binary code with black and white patterns increases, such as B2 to B10. In order to minimize errors during image scanning, the binary code will be converted to Gray codes of G1 to G10 using bitwise XOR operation.

3. Results and Discussions

3.1 Decoding depth transformation of 3D workpiece

Fig. 4 are the patterns of the sequential projections for decoding depth information (a) sequential column and row patterns of integrated Gray codes from low to high frequency

(b) converted logical values from single pixel with a strip of binary image (c) Gray codes to binary codes using bit-wise XOR operation for calculating real depth. In order to estimate the intensity levels of projected patterns, all projected sequences of column C_1 to C_{10} and the row R_1 to R_{10} directions are captured from the camera images and decoded from received bit sequences for each camera pixel.

The left of Fig. 4(a) is the sequence of projection versus horizontal spatial distribution projected 10 Gray patterns from low to high frequencies of 1 to 512 pairs per screen in the column directions. Each frame dimension of C_1 to C_{10} is 768 ×1024 pixels. Assign that a single pixel with sequence of C_1 to C_{10} projections for over time-code light patterns is shown in Fig. 4(b). Remarkably, the single pixel has a unique illumination of Gray code and has a Gray intensity value of 10 bits at over time-code patterns. A series of structured light patterns projected on the scene to label each pixel uniquely; the set of projected intensities is decoded in order to give each pixel a unique label. Therefore, each pattern image is a bit-plane of the Gray code for each column and row direction. For depth map of the scene, the Gray code patterns of the bit-plane are decoded into binary images computed using XOR operation as shown in Fig. 4(c). The depth level of each pixel is 1024 (10 bits) binary codification pattern. A decimal value of depth acquisition D for single pixel is calculated in column direction as eq. (5):

$$D = \sum_{n=1}^{10} C_n \times 2^{n-1} \quad (5)$$

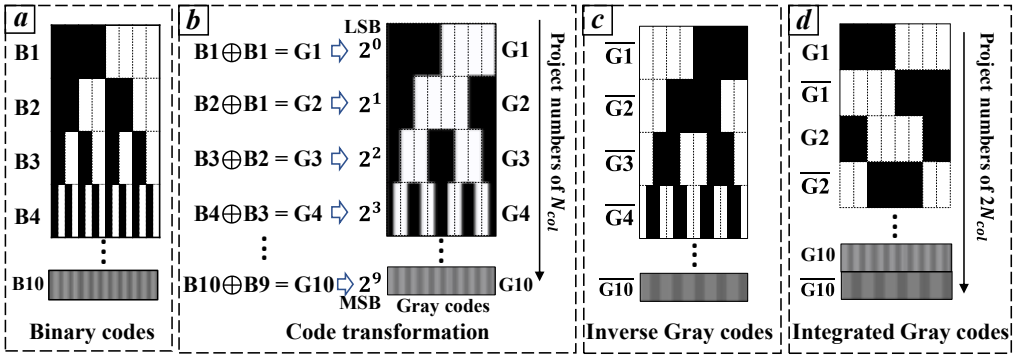


Fig 3. Projective procedures of structured light of the integrated Gray code in column direction based on (a) generated binary codes of B1 to B10, (b) bitwise XOR operation to form Gray codes of G1 to G10, (c) inverse Gray codes to form $\overline{G1}$ to $\overline{G10}$, and (d) integrated cross codes of G and $\bar{G}$.

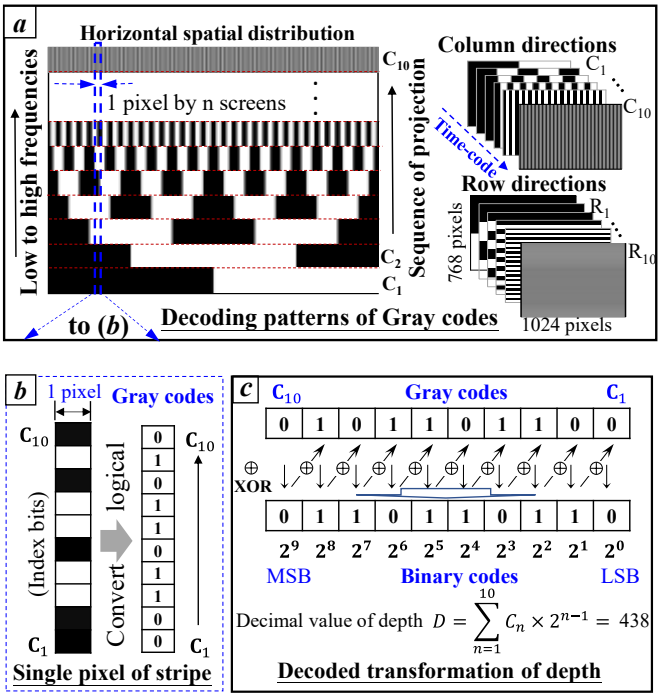


Fig. 4. Patterns of the sequential projections for decoding depth information (a) sequential column and row patterns of integrated Gray codes from low to high frequency (b) converted logical values from single pixel with a strip of binary image (c) Gray codes to binary codes using bit-wise XOR operation for calculating real depth.

For building a reliable scanning system, it is critical and important to note that the working distances, (WD), field of view (FOV), the minimum resolution of line-pair. The WD of the camera and the projector from the fronts of both lens to the top surface of the vise are 50 and 60 cm, respectively. The projected range of the mini projector on the horizontal level of vise top is 60 cm × 60 cm. The observable FOV range of the camera on the horizontal level of vise top is 60 cm × 60 cm. In general, there is high accuracy for setting tool offset when WD and FOV range are set as small as possible. For our system, the minimum observable resolution of line-pair projected Gray code pattern on the vise top is about 10 lp/mm. The minimum resolution of line-pair image captured clearly by camera is about 20 lp/mm. The different projective frequencies of 8 and 32 line-pair/screen in column direction and 16 and 64 line-pair/screen in row direction are shown in Fig. 5(a), 5(b), 5(c), and 5(d), respectively. The workpiece fixed on the vise is a high carbon steel with a dimension of 25.35 × 25.4 × 800 mm^3. The scanning procedures of the workpiece was used Gray structured light of column and row directions for automatically setting tool offset. Remarkably, each scene pattern clearly receives irradiance from a single scanning frequency for capturing images. The patterns projected on workpiece can be robustly binarized for depth information due to low inter-reflections, diffusion and sub-surface scattering.

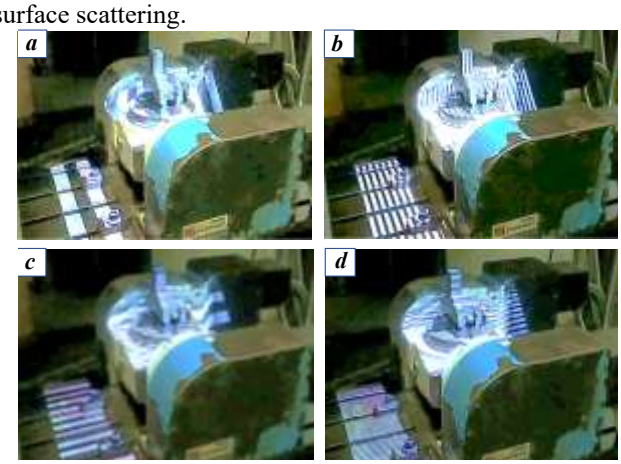


Fig. 5. showed partially scanning procedures of the workpiece using Gray structured light of column and row directions for automatically setting tool offset at different projected frequencies of (a) 8 and (b) 32-line pairs/screen in column directions (c) 16 and (d) 64-line pairs/screen in row directions.

3.2 Automatic alignment of workpiece position

This study employs structured light technology to construct a 3D point cloud model of the workpiece, as shown in Fig. 6. As shown in the result, the reconstructed geometry

clearly represents the main structure of the target object, and the region of interest is highlighted by the red bounding box, as shown in Fig. 7. The overall point cloud distribution demonstrates good geometric consistency, indicating that the calibrated relationship between the projector and camera system is stable and capable of accurately mapping 2D image coordinates into 3D spatial information. In terms of modeling characteristics, structured light provides high-density surface sampling, enabling detailed reconstruction of the object geometry. The captured point cloud effectively preserves the planar features and boundary contours of the workpiece, which is essential for downstream applications such as pose estimation and automatic alignment in CNC machining systems. The continuity of the reconstructed surface further indicates that the depth recovery process is reliable and maintains spatial coherence without significant distortion.

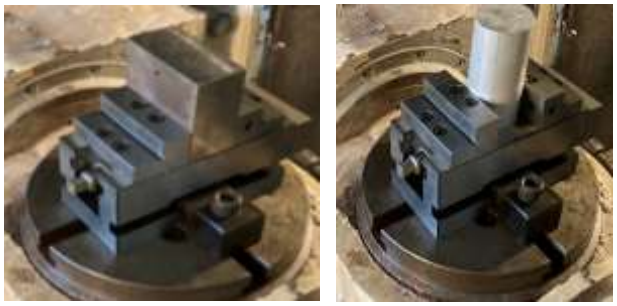


Fig. 6. Different workpieces for automatic alignment position based on structured light scanning.

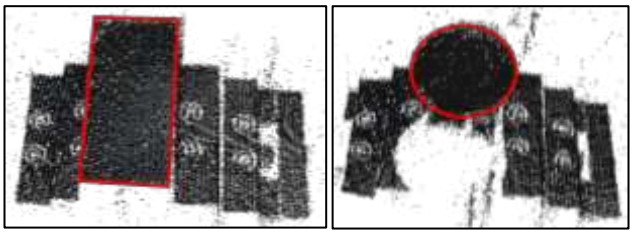


Fig. 7. Reconstructed geometry mapping from 2D image coordinates into 3D spatial information for automatic alignment in CNC machining systems.

The extraction of the geometric center from a point cloud is a fundamental step in object localization and pose estimation, as shown in Fig. 8. Its accuracy and performance are characterized by statistical robustness and noise suppression. The geometric center, typically calculated as the centroid of the point set p, is inherently robust against random sensor noise. Since the center is a statistical result of the entire point population, the influence of individual stochastic outliers is significantly minimized, leading to higher spatial repeatability compared to single-point measurements. For geometric symmetry and sampling uniformity, the stability of the center point depends heavily on the uniformity of the point distribution. For symmetric objects, a uniform sampling density ensures that the calculated centroid aligns precisely with the theoretical geometric center. Any bias in point density will cause a proportional shift in the estimated center.

The effectiveness of the proposed automatic alignment system was evaluated by measuring the positioning errors in the X, Y, and Z axes across ten independent experimental trials. After 3D scanning and geometric center calculation, the workpiece was automatically aligned to its target position. The deviations between the calculated center and the ground truth are illustrated in Fig. 9. As shown in the experimental results, the positioning errors in all three axes remain within a highly stable range. The X-axis errors (represented by black squares) fluctuate between -0.06 mm and -0.10 mm, with an average deviation of approximately -0.084 mm. The Y-axis errors (red circles) exhibit the highest stability among the three dimensions, with values closely clustered around the mean of -0.065 mm. In contrast, the Z-axis errors (blue triangles) show a positive bias, ranging from 0.05 mm to 0.10 mm, with an average error of 0.072 mm. The consistency of the error patterns—specifically the relatively constant offsets observed in the X and Y-avg lines—suggests that these are likely systematic errors stemming from the initial system calibration or the mechanical tolerances of the alignment stage. The Z-axis exhibits slightly higher variance compared to the XY plane, which can be attributed to the inherent depth resolution limits of the structured-light 3D scanning process and the sensitivity of center-fitting algorithms to surface point cloud noise.

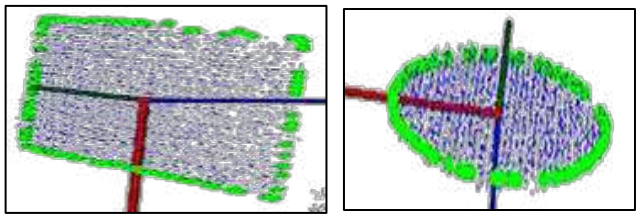


Fig. 8. Extraction of the geometric center from 3D cloud for automatic alignment in CNC machining systems

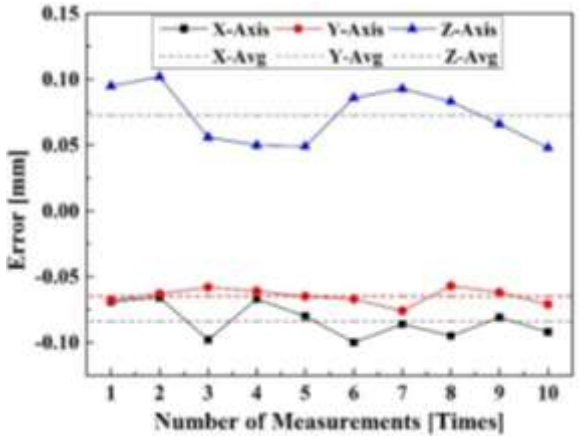


Fig. 9. Positioning errors in X, Y, and Z after 3D scanning and calculating centers using camera and projector.

The positioning accuracy of the object center was evaluated to verify the performance of the proposed automatic alignment system. Fig. 10 illustrates the deviation of the calculated center from the target position in the X, Y, and Z axes across ten repetitive measurement cycles. The experimental results demonstrate that the positioning errors for all three dimensions are significantly minimized and fluctuate within a narrow range of ± 0.05 mm. Specifically, the Y-axis (red circles) shows the highest stability, with most errors concentrated within ±0.01 mm, indicating exceptional repeatability in this direction. The X-axis (black squares) and Z-axis (blue triangles) exhibit slightly higher fluctuations, with maximum deviations of approximately 0.03 mm and -0.045 mm, respectively. The fact that the total positioning error remains well below 50 um proves that the system is highly reliable for precision manufacturing tasks. The convergence of errors near zero confirms that the 3D scanning and center-calculation algorithm can accurately track and adjust the workpiece position. This sub-millimeter precision ensures that the automatic alignment system meets the stringent requirements for high-end assembly and inspection processes.

4. Conclusion

This study successfully develops an automated workpiece alignment system by integrating 3D structured light scanning with CNC machining processes. By leveraging gray-code

reconstruction and point cloud edge detection, the system effectively eliminates the risks associated with manual probe handling and human error. With a demonstrated dimensional accuracy of ±0.1 mm and a positioning precision within 0.05 mm, the proposed method provides a robust and reliable solution for enhancing machining consistency and operational safety in industrial environments.

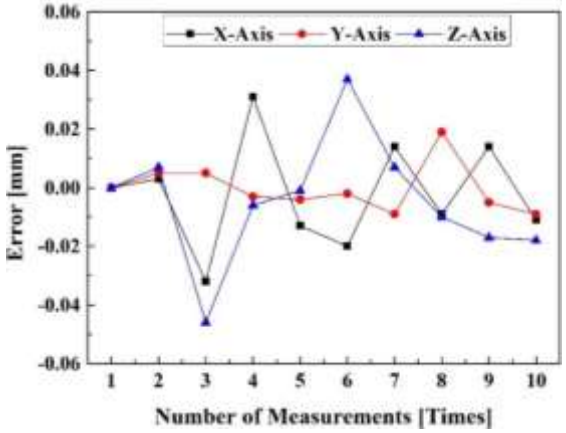


Fig. 10. Floating value of the positioning center for the automatic alignment system for automatic modeling workpiece

The establishment of a precise workpiece coordinate system remains a cornerstone of successful CNC machining. As modern manufacturing shifts toward higher degrees of automation and precision, the limitations of traditional manual probing—characterized by high dependency on skilled labor and susceptibility to human error—have become increasingly prominent. This research addresses these critical challenges by introducing an innovative automatic calibration system that integrates 3D structured light scanning with machine home position alignment, marking a significant step forward in intelligent manufacturing. The core contribution of this study lies in the seamless fusion of Gray-code-based structured light reconstruction and optical probing. By capturing the 3D geometry of the workpiece directly at the machine home position, the system generates a high-fidelity digital twin that allows for the precise identification of edge coordinates. This approach not only streamlines the setup process but also provides a non-contact preliminary assessment that protects expensive machine components and probes from potential damage caused by manual input errors. The integration of 3D modeling and structured light scanning provides a reliable, accurate, and efficient solution for automatic workpiece coordinate setting. This research not only validates the feasibility of using optical reconstruction for CNC alignment but also offers a scalable model for future developments in smart machining centers. Future work may explore the integration of AI-driven feature recognition to further enhance the system's versatility across even more complex workpiece geometries.

5. Acknowledgments

This work was partially supported by the Ministry of Science and Technology, under Grant Nos. NSTC 113-2221-E-150-010 and NSTC 114-2221-E-150-050, and Smart Machine and Intelligent Manufacturing Research Center.

Declarations

Competing interest. The authors declare that they have no known competing financial interests or personal relationships that could have appeared to influence the work reported in this paper.

References

[1]. S. Rakic, M. Pavlovic, and N. Zivlak, "Advancements in Smart Manufacturing and Industry 4.0: A Comprehensive Review," Applied Sciences, 2025.

[2]. M. Soori, B. Arezoo, and R. Danyi, "Industry 4.0 enabled sustainable manufacturing and digital twins: A review," Sustainability, 2025.

[3]. J. J. Aguilar et al., “Stereo vision for 3D measurement: accuracy analysis and industrial applications,” Measurement, 1996.

[4]. R. J. Valkenburg and A. M. McIvor, “Accurate 3D measurement using a structured light system,” Image Vis. Comput., 1998.

[5]. J. Meza et al., “Triangulation approaches for structured light systems,” Proc. SPIE, 2020.

[6]. G. Sansoni, M. Trebeschi, and F. Docchio, “State-of-the-art and applications of 3D imaging sensors in industry,” Sensors, 2009.

[7]. C. Chen, N. Gao, and Z. Zhang, “Simple calibration method for dual-camera structured light system,” J. Eur. Opt. Soc., 2018.

[8]. J. Zhang, L. Yang, and H. Wang, "Calibration method for event-based structured light systems using DLP strobe-stripe fields," Measurement, 2026.

[9]. Y. Liu, X. Chen, and Z. Jiang, "Deep Learning-Based Trajectory Planning for Reflective Workpiece Automation in Industrial Inspection," ScienceDirect - Mechanical Systems and Signal Processing, 2025.

[10]. X. B. Chen et al., “Accurate calibration for a camera–projector measurement system based on structured light projection,” Opt. Lasers Eng., 2009.

[11]. C. Chen, N. Gao, and Z. Zhang, “Simple calibration method for dual-camera structured light system,” J. Eur. Opt. Soc., 2018.

[12]. S. Yamazaki, M. Mochimaru, and T. Kanade, “Simultaneous self-calibration of a projector and a camera using structured light,” IEEE CVPR Workshops, 2011.

[13]. M. E. Deetjen and D. Lentink, “Automated calibration of multi-camera-projector structured light systems,” Opt. Express, 2018.

[14]. H. Li, Q. Zhang, and X. Wu, "An Improved Projector Calibration Method by Phase Mapping Technology for Structured Light Systems," Sensors, 2023.

[15]. K. Tanaka and S. Hashimoto, "Efficient and accurate projector calibration based on automated board detection and feature extraction," Heliyon, 2023.

[16]. T. No et al., “Cutting force and stability for machining using structured light metrology,” Procedia CIRP, 2020.

[17]. T. Wang, J. Smith, and L. Garcia, "Comparative Evaluation of 3D Reconstruction Methods for Object Pose Estimation in Industrial Environments," arXiv preprint (Computer Vision and Pattern Recognition), 2024.

[18]. R. Anderson, M. Taylor, and D. Lee, "Three-dimensional unsupervised probabilistic pose reconstruction (3D-UPPER) for complex geometries," Scientific Reports, 2023.

[19]. C. H. Huang, S. J. Lin, and Y. C. Chen, "3D Scanning System of Structured Light for Aiding Workpiece Position of CNC Machine Tool," IEEE Transactions on Industrial Informatics, 2023

[20]. P. Kowalski and J. Marek, "Accuracy of the New Method of Alignment of Workpiece Using Structural-Light 3D Scanner," Journal of Machine Engineering, 2023.